NONDESTRUCTIVE TESTING AND EVALUATION
2024, VOL. 39, NO. 8, 2486–2509
https://doi.org/10.1080/10589759.2024.2304257

Taylor & Francis
Taylor & Francis Group

Check for updates

Predicting compressive strength of quarry waste-based geopolymer mortar using machine learning algorithms incorporating mix design and ultrasonic pulse velocity

Navaratnarajah Sathiparan[a] and Pratheeba Jeyananthan[b]

[a]Department of Civil Engineering, Faculty of Engineering, University of Jaffna, Kilinochchi, Sri Lanka; [b]Department of Computer Engineering, Faculty of Engineering, University of Jaffna, Kilinochchi, SriLanka

ABSTRACT
The current study aimed to investigate the possibility of predicting the compressive strength of geopolymer mortar by mix design parameters, ultrasonic pulse velocity (UPV) and machine learning techniques. Here the geopolymer mortar is produced from eggshell ash and rice husk ash as precursors, NaOH solution as activator and quarry waste as fine aggregate. Twenty-seven combinations of geopolymer mix and a total of 189 mortar cubes were cast and tested for UPV and compressive strength. Seven different machine learning techniques were used to predict the compressive strength assessment tools: linear regression, artificial neural networks, boosted tree regression, random forest regression, K-Nearest Neighbor, support vector regression and XGboost. Among the diverse machine learning models evaluated in this study, XGboost exhibited remarkable efficacy in forecasting the compressive strength of geopolymer mortar. The investigation conducted using SHAP indicates that the concentration of UPV shows the most substantial influence on the prediction of compressive strength.

ARTICLE HISTORY
Received 15 September 2023
Accepted 2 January 2024

KEYWORDS
Geopolymer; machine learning; UPV; eggshell ash; rice husk ash

1. Introduction

The utilisation of alternative materials for cement and river sand in masonry blocks is gaining popularity due to environmental concerns and the need for sustainable construction practices. The manufacturing process of cement involves excessive energy and CO_2 emissions. The excessive extraction of river sand has notable ecological consequences, including deepening river beds, intensified soil erosion, reduced water table levels, and the depletion of aquatic biodiversity within water bodies [1,2].

There is an emerging inclination towards the utilisation of quarry waste as a viable alternative to natural sand in the production of construction materials. Quarry waste is a residual generated during the process of rock-crushing, which contributes to the exacerbation of environmental concerns and poses potential risks to human health. The utilisation of quarry waste in cementitious materials presents a promising approach to significantly mitigate or maybe eradicate these issues. The substitution of quarry waste for natural sand in construction materials presents a viable solution for addressing the issue

CONTACT Navaratnarajah Sathiparan sakthi@eng.jfn.ac.lk

of waste accumulation, while concurrently enhancing the sustainability of these materials. Furthermore, the utilisation of quarry waste in construction materials has various benefits, including reduced cement consumption, which enhances the strength of cementitious materials, and its environmentally benign nature [3]. According to Shen et al. [4] and Goncalves et al. [5], it has been observed that the water needed for achieving consistent workability of fresh mortar is higher when using quarry dust as opposed to river sand. However, in direct comparison to concrete produced with an equivalent quantity of river sand, concrete constructed from quarry refuse has greater strength [6]. A like pattern was observed in the literature published on self-compacting concrete [7–9]. According to Sundaralingam et al. [10], it has been asserted that a greater water-to-cement ratio is necessary to maintain the appropriate workability of the cement-sand mortar. The setting time and water retention capacity of fresh cement-sand mortar were shown to improve with the inclusion of quarry waste content, as reported in a study [11]. Furthermore, it has been observed that the inclusion of quarry waste in the hardened mortar leads to a rise in sorption, water absorption and drying. Nevertheless, it was detected that the presence of quarry waste material led to a rise in both compressive and flexural strength of the mortar.

Conversely, researchers have examined the application of geopolymer technology in the production of masonry units to completely replace cement. The present technology can significantly transform the construction sector through the provision of an alternative to conventional concrete blocks, hence promoting sustainability and environmental friendliness. The formation of geopolymer gel is achieved through the alkali activation process, wherein the interaction between aluminate and silicate-rich fly ash takes place in the presence of alkaline activator solutions [12]. In the 1980s, Davidovits and Sawyer [13] made notable contributions to the field of cement technology by the introduction of the initial geopolymer cement. This significant advancement afterwards facilitated the progress of pyrament cement or slag-based geopolymer cement creation. The year 1997. Silverstrim et al. [14] and Van Jaarsveld et al. [15] effectively developed a geopolymer cement by utilising fly ash as a predominant constituent. In recent times, there has been a growing utilisation of fly ash-based geopolymer techniques for the manufacturing of various structural components and construction materials. The aforementioned options encompass [16–18], concrete blocks [19], earth walls [20], walling materials [21–23], recycled concrete [24], and ceramics [25].

While the predominant area of investigation in geopolymerization study has centred around aluminosilicate gel as the fundamental binding agent, few scholarly inquiries have delved into the utilisation of eggshell powder or rice husk ash as alternative precursors [26]. The existing research has primarily concentrated on the application of supplementary cementitious materials, such as rice husk ash or eggshell powder, in combination with metakaolin, fly ash, and granulated blast furnace slag, as a primary component in the production of cementitious materials [27–33].

The essential criterion of importance is the compressive strength (f_c) of this particular type of mortar. Typically, the assessment and prediction of the f_c of construction materials relies on experimental testing (both destructive and non-destructive), mathematical modelling, and machine learning algorithms. Destructive testing is a valuable methodology due to its ability to generate replicable outcomes. Nevertheless, to be deemed valuable, strict control measures must be implemented. The outcomes achieved can be subject to modification due to various internal or external influences. Additionally, the process of destructive testing entails the examination of an extensive quantity of materials, resulting in the utilisation of increased energy, time, and material resources. Hence, it might be argued that there is a lack of cost-effectiveness [34]. Non-destructive testing (NDT) offers a viable approach for the estimation of f_c of the materials. The NDT is a testing methodology that possesses the capability to assess material qualities without causing any damage or alteration to the sample under examination. A variety of NDTs have been established to assess the quality of construction materials [35–38]. Several methods, including UPV and rebound hammer, are commonly employed for assessing material properties. Among these approaches, UPV has been found to offer more precise predictions [39–42]. The UPV measurement used for prediction of compressive strength and other characteristics of construction materials such as concrete [43,44], cement mortar [45,46], stabilised earth blocks [47], rocks [48–52], etc. Nevertheless, the majority of the existing research has mostly concentrated on the application of these techniques in concrete. However, there is limited research in the evaluation of the quality of geopolymer mortar using NDT methods.

Mathematical equations offer a convenient and efficient method for determining f_c. Nevertheless, the effectiveness of these models is contingent upon the quality of the data utilised in their creation. If the data does not accurately reflect the prevailing conditions, the prognostications may lack precision. Machine learning (ML) models can offer precise predictions of f_c. Additionally, these models can acquire knowledge from new data and enhance their predictive capabilities through iterative refinement. The ML techniques have gained widespread usage in the prediction of construction material characteristics [53–55]. The ML has been identified as a highly efficient method for predicting the characteristics of construction materials, as these qualities are influenced by several variables [56,57]. In addition, a range of ML methods have been employed in the prediction of the f_c of construction materials [58–60]. Several scholarly investigations have employed a fusion of non-destructive testing techniques, specifically UPV data, in conjunction with ML methodologies to predict the characteristics of construction materials [57], notably concrete [61–64]. Nevertheless, the current body of literature lacks sufficient study on the utilisation of UPV and ML approaches for accurately forecasting the compressive strength of geopolymer mortar ($f_{c\text{-}gpm}$).

Hence, the principal objective of this study is to predict the $f_{c\text{-}gpm}$ by employing UPV measurement with ML approaches. This approach allows for the evaluation of geopolymer mortar quality without inducing any material damage. Twenty-seven distinct combinations of ESA, RHA, and NaOH concentration with quarry waste as fine aggregate were utilised in the production of the geopolymer mortar. The study investigated the associations among mix design, UPV, and $f_{c\text{-}gpm}$ through the application of multiple ML approaches. The outcome of the study shows that with the use of machine learning algorithms, the mechanical properties of geopolymer mortars in different combinations of ESA, RHA, caustic soda and UPV become predictable. So, material scientists and designers could choose the best mix design to achieve the desirable properties of geopolymer mortar for the particular application.

2. Materials and methods

2.1. Materials used

Figure 1 depicts the particle size distribution and physical characteristics of the raw materials used in the formulation of the mortar. The collection of eggshells was conducted at several restaurants situated in Kilinochchi, a locality within the Northern Province of Sri Lanka. These eggshells were initially washed in clean water and exposed to sunlight for drying. The dry eggshells were crushed using a hammer mill and then sieved via a screen having a mesh size of 1 mm. The eggshell powder was then treated to calcination at a temperature of 700°C for a period of three hours inside a furnace, leading to the formation of eggshell ash (ESA). The choice of the calcination temperature and time was calculated based on the current literature [30,65–67].

The RHA used in this study was obtained from a kiln located in Paranthan, a geographical area situated within the Northern Province of Sri Lanka. The kiln used an elevated temperature of 650 °C to thermally decompose rice husk, which functioned as the only fuel substrate for the oxidative reaction. The RHA acquired from the kiln was free from any other substances. The RHA that was acquired was thereafter submitted to sifting using a 2.36 mm screen, and the fraction that successfully passed through the sieve was gathered to conduct tests. The quarry debris used in this investigation was obtained from a manufacturing company located at Divulapitiya, situated in the Western area of Sri Lanka. In this study, commercially available caustic soda was used as sodium hydroxide (NaOH).

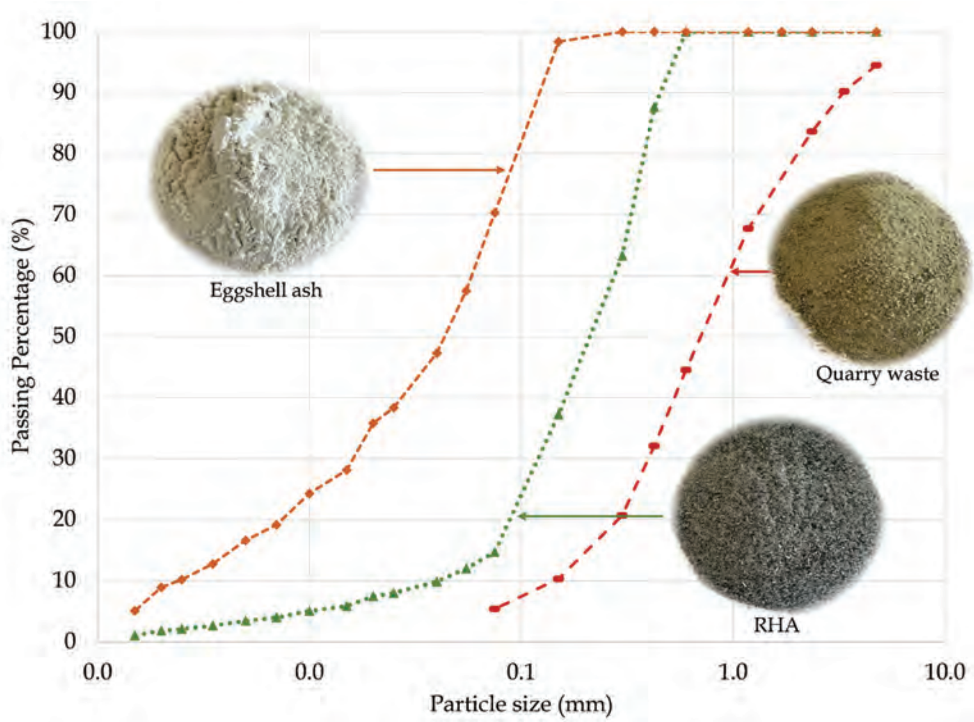

Figure 1. Particle size distribution and physical appearance of the raw materials used for the mortar mix.

Table 1. Physical characteristics and chemical composition of the raw materials.

	Cement	RHA	ESA	QW
Physical properties				
Specific gravity	3.15	1.80	1.25	2.34
Bulk density (kg/m^3)	1362	235	305	1641
Fineness modulus				2.97
Chemical composition (%)				
SiO_2	20.60	91.04	0.04	66.76
Al_2O_3	4.51	0.38	0.01	19.20
Fe_2O_3	3.62	0.45	0.01	3.62
CaO	66.55	0.61	74.60	3.81
MgO	1.17	0.29	0.25	1.64
P_2O_5	-	0.33	0.28	-
Na_2O	0.40	0.97	0.13	1.27
K_2O	0.39	1.89	0.05	2.16

Table 1 presents a comprehensive depiction of the chemical composition and physical characteristics of the raw materials. Calcium oxide is the predominant component in both cement and ESA, accounting for 66.5% and 74.6% of their respective compositions. Silica oxide constitutes 91% of the content of RHA. Calcium and silica oxide play a crucial role in the development of strength throughout the hydration process.

2.2. Mix design and specimen preparation

Figure 2 shows the diverse mixture proportions used in the current investigation. The water-to-quarry waste ratio used in all the mixtures remained constant at 0.15, as reported in the relevant literature [10,11]. The amounts of ESA, RHA, and NaOH included in the mixture were calculated based on the weight per kg of quarry waste. This research included three discrete proportions of materials, including different quantities of ESA and RHA, which ranged from 25 g to 75 g, rising in 25 g intervals. Similarly, the quantity of NaOH ranged from 20 g to 40 g, increasing by increments of 10 g.

During the process of block preparation, the appropriate quantity of water was used to dissolve the NaOH flakes. Following this, a thorough integration of the precursor substances, namely ESA and RHA, together with quarry waste during the desiccation phase was carried out. Subsequently, the aqueous state of the NaOH solution was amalgamated with a pre-existing, desiccated blend. The precursor materials, including quarry refuse, were manually blended with a NaOH solution until a homogeneous mixture was achieved. The test cubes were manufactured using a sequential process of pouring the wet liquid into the moulds in three separate levels. The compaction procedure included hand application to each layer using a tamping rod, with 10 strokes used for each layer. The dimensions of the cube were 50 mm × 50 mm × 50 mm, and it was cast according to the ASTM C109 standard [68]. A total of seven cubes were manufactured for each mix identification. The cubes were exposed to a curing procedure at ambient temperature for a duration of 28 days before the commencement of the testing. Figure 3 illustrates the visual characteristics of the selected mortar cubes after a 28-day curing period. When the content of ESA, RHA and NaOH content in the mix is increased, the resulting colour gets darker.

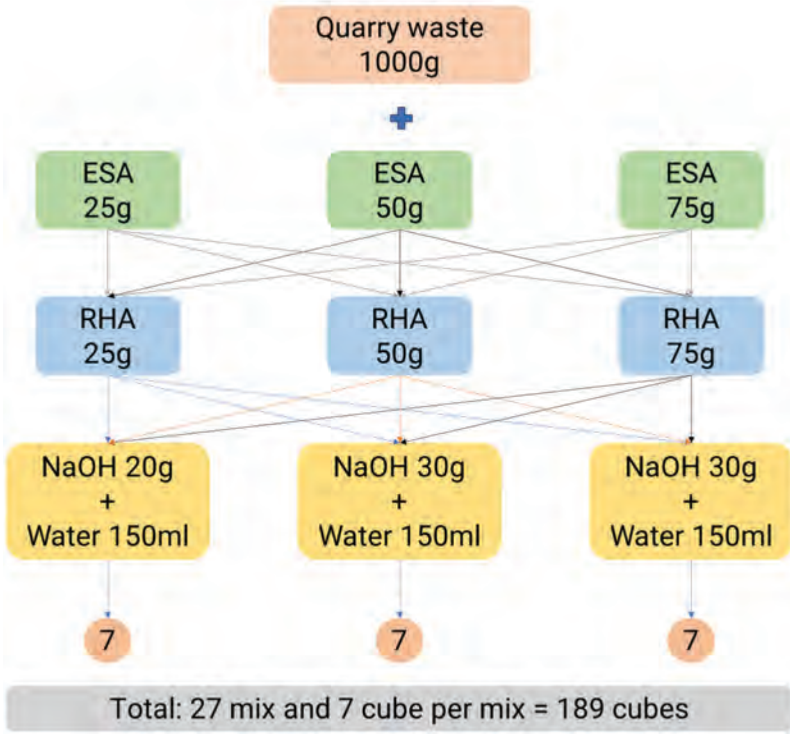

Figure 2. Outline of the mix proportion used for the mortar and it describes the amount of ESA, RHA, NaOH and water added for the one kg of quarry waste.

2.3. Testing

2.3.1. Ultrasonic pulse velocity measurement

The UPV of geopolymer mortar was measured utilising a portable ultrasonic NDT digital indication tester, following the ASTM C597 [69]. The PULSONIC model 58-E0046/5, an ultrasonic pulse analyser, is employed to quantify the UPV. The arrangement of the equipment is depicted in Figure 4. The gadget under consideration is a portable instrument designed to quantify the velocity of ultrasonic pulses within various materials [70]. It possesses a transit time range of 16 milliseconds, a sampling rate of 2 megahertz, a resolution of 0.1 seconds, and a transmitter output of 1200 volts. The UPV measurements in this investigation were conducted using a frequency of 54 kHz, as it has been determined to be more appropriate for assessing block attributes [71]. Before the commencement of the experiment, the equipment underwent calibration utilising a reference bar with a measurement of 25.4 µs. Vaseline was employed as a couplant to enhance the level of contact between the surface of the block and the transducer. The transducers were carefully placed in close contact with the two opposing surfaces of the blocks until a consistent transit time was observed. In the present study, longitudinal wave velocity was used to measure the ultrasonic pulse velocity. The captured data included the distance covered by the ultrasonic wave and the pulse transit time. Measurements of ultrasonic pulse velocity (UPV) were conducted in three orientations: one aligned with the direction of compaction, and the other two perpendicular to it. The

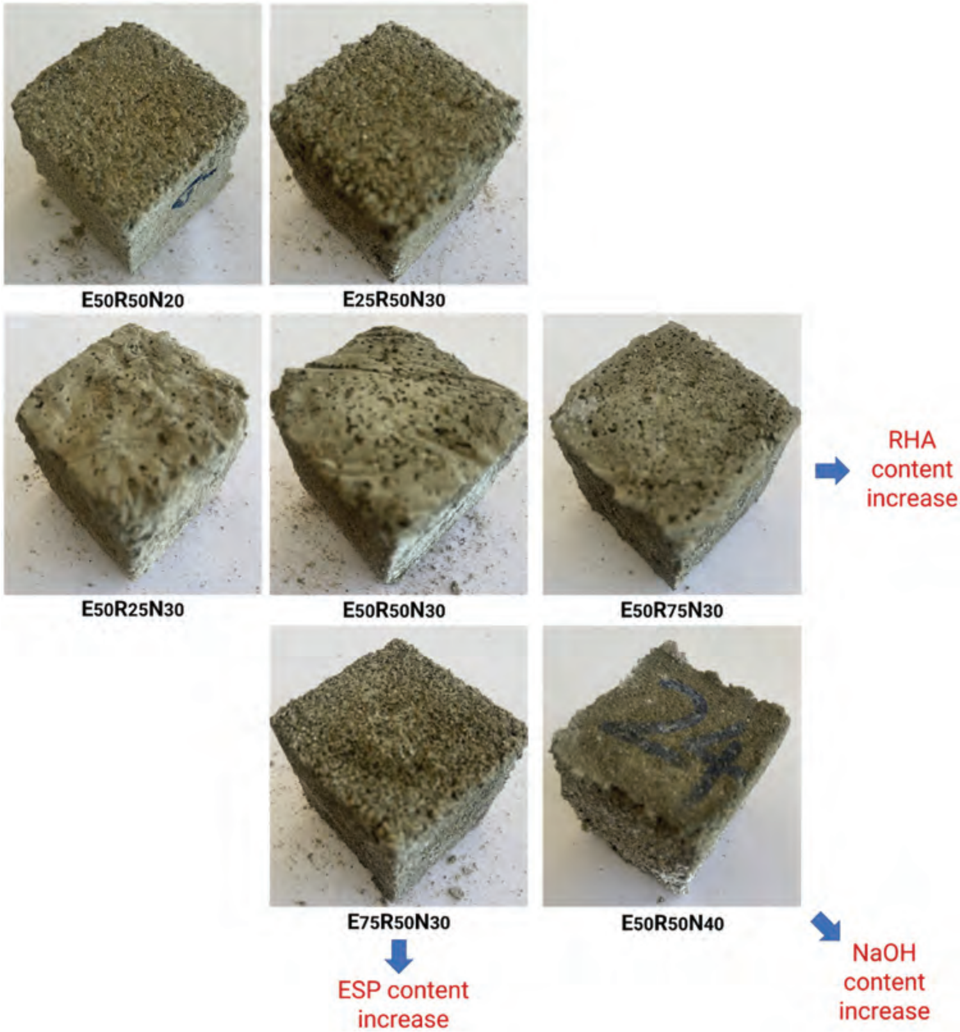

Figure 3. The visual appearance of selected geopolymer mortar cubes used in the present study. Figure provides the overview of how colour changes, when the content of ESA, RHA and NaOH is increased in the mortar.

Figure 4. The measurement of UPV of mortar cube and measuring instrument.

average of these measurements is denoted as UPV. A total of 189 cubes were utilised for both ultrasonic testing and mechanical testing. The UPV was calculated by using Equation (1).

$$\mathrm{UPV} = \mathrm{L}/\mathrm{t} \tag{1}$$

where, UPV in km/s, width of the cube (L) in km, and transit time (t) in sec.

2.3.2. Compression test

The compression test was conducted with a Universal Testing Machine (UTM) through the displacement control technique following the guidelines stated in ASTM C109 [68]. The test employed cubes with dimensions of $50 \times 50 \times 50\ \mathrm{mm}^3$. The cubes were subjected to a uniaxial load at a rate of 1 mm/min. for testing purposes. For each mix, seven cubes were subjected to compression testing at 28 days for each mix. The mean compressive strength of each set of cubes was found by calculating the average of the related measurements of strength. The computation of compressive involved determining the ratio between the ultimate load applied and the area of the bed face [72,73].

2.4. Machine learning modeling

Figure 5 depicts the flowchart illustrating the implementation of the ML model for the prediction of the $f_{c\text{-gpm}}$ in the present investigation. In a general sense, there are five primary phases as outlined below:

Step 1 - Preparation of the dataset: In this stage, the input data, namely ESA content, RHA content, NaOH content, UPV, and the response variable of $f_{c\text{-gpm}}$, were gathered from the experimental programme to construct the ML models. The dataset consists of a total of 189 observations. It was divided into two groups using random allocation. Specifically, two-thirds of the datasets were used for training the ML model, constituting the training dataset. The remaining one-third of the dataset was reserved for evaluating the performance of the ML model, forming the testing dataset.

Step 2 - Training of the ML models: In this stage, all suggested ML models were trained using the training dataset. A total of seven techniques were used in the training of ML models. These algorithms include artificial neural network (ANN), boosted decision tree (BDT), K-nearest neighbours (KNN), linear regression (LR), random forest regression (RFR), support vector regression (SVR), and XGboost models. Seven different machine learning algorithms have employed to identify which one gets the best accuracy in predicting compressive strength, using the optimum attributes found by various feature selection approaches. Five-fold cross-validation was utilised in a grid search to optimise the hyperparameters of the machine learning algorithms prior to their implementation. Considering the large number of possible combinations, the analysis has largely focused on the hyperparameter ranges that are frequently reported. The range of hyperparameter values and the ideal value for the machine learning technique employed in the current investigation are summarised in Table 2. To minimise the risk of overfitting, the R^2 and RMSE values were used to evaluate each model's performance on both the training and test datasets. Various categorisation models were employed to ascertain the most precise outcomes.

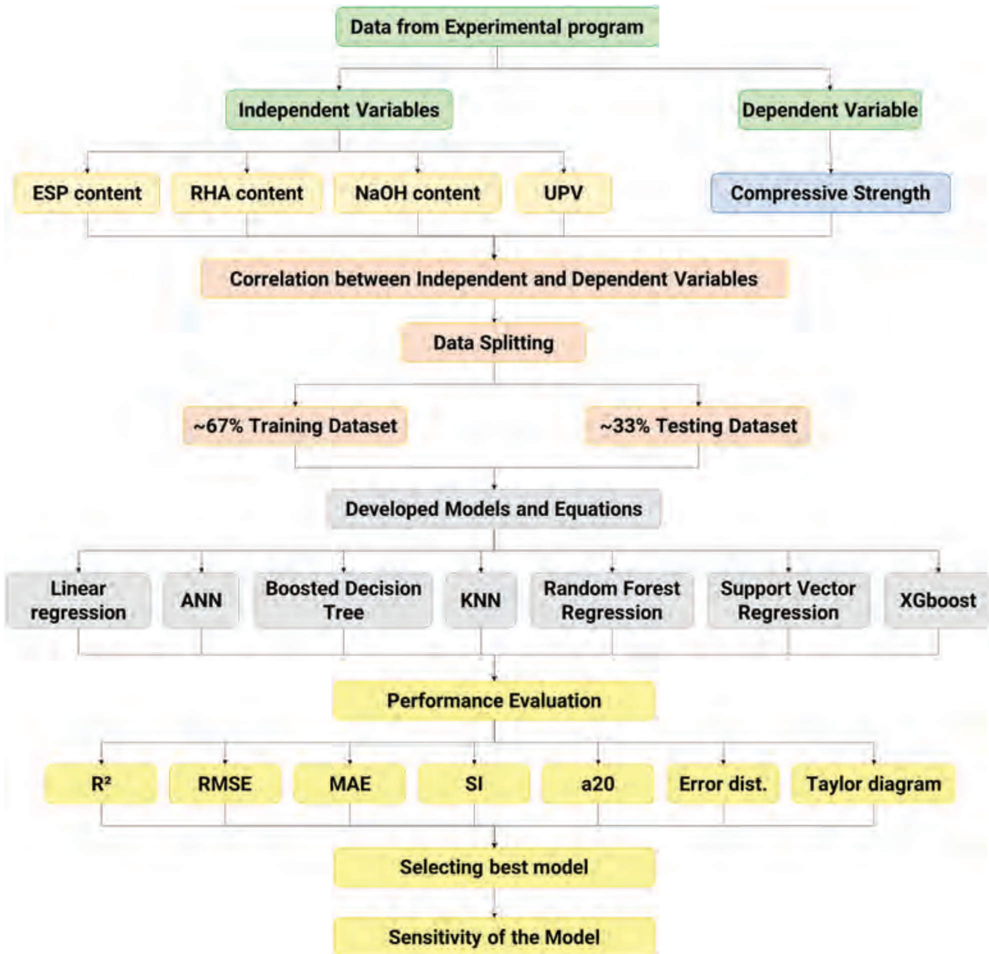

Figure 5. Proceedings of ML modelling include the independent and dependent variable, data splitting technique, various machine learning techniques used in the present study, performance indicators and sensitivity of the model for the best machine learning model.

Step 3 - Validation of the ML models: In this stage, the testing dataset was used to verify the ML models in step 2.

Step 4 - Performance comparison of the models: Initially, the outcomes derived from the ML models' predictions were compared with the factual experimental findings. Subsequently, all ML models underwent evaluation using five statistical metrics, namely R^2, RMSE, MAE, SI, and a20-index [74,75]. Scatter index is calculated by dividing RMSE with mean of the observation's values. The α20-index is a new measure for assessing the reliability of the soft computing techniques developed, as calculated by dividing number of data points with a predicted strength to experimental strength ratio between 0.80 and 1.2 with number of data points [76,77].

Furthermore, the evaluation of ML models' performance involves the use of two specific criteria, namely error distribution and Taylor diagram. These criteria are employed to evaluate the effectiveness of the models. The determination of this error involves the calculation of the disparity between the predicted and

Table 2. Hyperparameter for ML algorithm.

Algorithm	Hyperparameter used	Analysed values
ANN	Number of layers: 1	[1,2]
	Nodes per layer: 3	[2,4,6,8,10]
BDT	Number of layers: 150	[100, 125, 150, 175, 200]
	Split per tree: 2	[2,4,6,8,10]
	Learning rate: .077	[0.01–0.1]
KNN	K = 3	[1–10]
RFR	Number of trees: 100	[50], 100, 200]
	Number of terms sampled per split: 3	[2–6]
	Number of terms: 4	[2,4,6,8]
	Minimum splits per tree: 10	[2,5,10]
	Minimum size split: 5	[2,5,10]
SVR	Kernel: Radial basis function	[linear, Radial basis function]
	Cost: 1	[0.1, 1, 10]
	Gamma: .25	[0.50, 0.25, 0.10, 0.01]
XGboost	Max_depth: 3	[1–10]
	Subsample: 1	[0.5–1]
	Colsample_bytree: 1	[0.5–1]
	Min_child_weight: 1	[1–5]
	Alpha: 0	[0–1]
	Lambda: 1	[0–1]
	Learning rate: .1	[0.1, 0.01, 0.001]
	Iterations: 30	[1–40]

experimental $f_{c\text{-gpm}}$. The Taylor diagram is a useful tool for evaluating the precision and dependability of these models. The Taylor diagram, a statistical instrument, offers a visual framework for the assessment and comparison of many models. The provided visual depiction demonstrates the level of concurrence between each model and the reference data, as assessed using correlation, standard deviation, and RMSE measures.

Step 5 - Sensitivity analysis: The SHAP analysis method was used to evaluate the significance and impact of the input parameters on the $f_{c\text{-gpm}}$.

3. Experimental results

Figure 6(a) depicts the UPV of geopolymer mortar. The results indicated that the UPV increased with higher NaOH concentration. The NaOH increases the reaction between ESA and RHA and generates enough cement paste to integrate the aggregate particles. Therefore, mortars become denser and it increases the velocity of the wave through solid particles. Although there is no clear trend between UPV and ESA or RHA content, generally increase in RHA content negatively influences the UPV of the mortar.

The graph depicted in Figure 6(b) illustrates the $f_{c\text{-gpm}}$. The results demonstrate that the NaOH content was highly influenced $f_{c\text{-gpm}}$ as a significant strength increase was observed between mortar with 30 g NaOH compared with 20 g NaOH per kg quarry waste. Generally, an increase in RHA content slightly decreases the strength and there is no clear trend between change in ESA content and $f_{c\text{-gpm}}$.

As shown in Figure 7, there is a correlation between UPV and $f_{c\text{-gpm}}$, which means that the higher the UPV, the higher the $f_{c\text{-gpm}}$. The results suggested an empirical equation to relate UPV and $f_{c\text{-gpm}}$ based on experimental data by following the formula given in Equation (2):

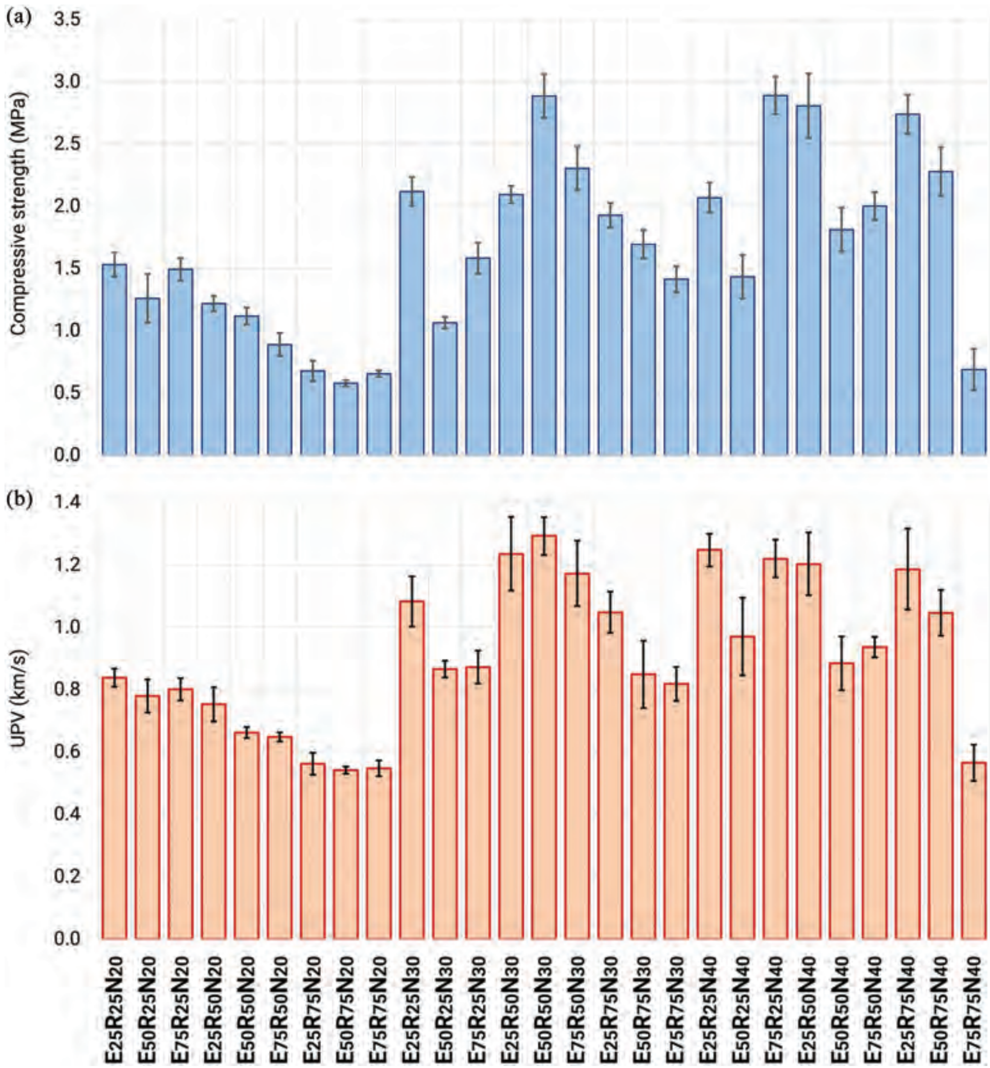

Figure 6. The variation of (a) UPV and (b) compressive strength of geopolymer mortar.

$$f_{c-gpm} = 2.6312\,UPV - 0.7251 \tag{2}$$

where $f_{c\text{-gpm}}$ in MPa and UPV in km/s. This formula can be used to estimate the $f_{c\text{-gpm}}$ from UPV test results. The coefficient of correlation (R^2) is equal to 0.8327, which indicates that there is moderate accuracy when $f_{c\text{-gpm}}$ is predicted from UPV. Therefore, this correlation depends on various factors such as the mix proportion.

4. Prediction using machine-learning models

The performance indicators for predicting $f_{c\text{-gpm}}$ by various ML algorithms are presented in Table 3, encompassing both the training and testing datasets. Figure 8 depicts the visual representation of the predicted and measured $f_{c\text{-gpm}}$ values for both the training and test datasets.

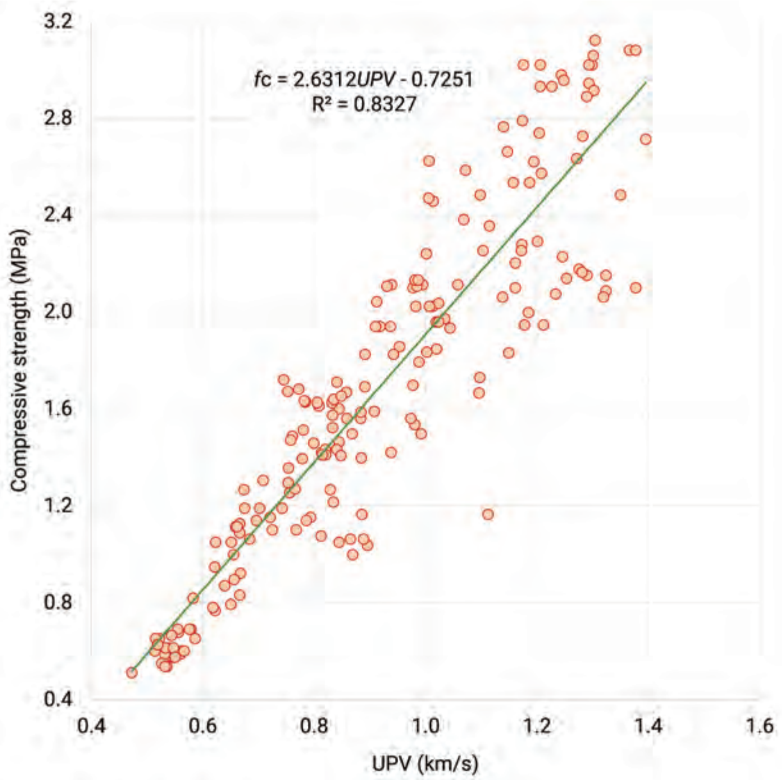

Figure 7. The relationship between UPV and compressive strength of geopolymer mortar. The continuous line best-fit line for the correlation between compressive strength and UPV.

Table 3. Performance indicators for training and testing datasets of various ML models for $f_{c\text{-gpm}}$.

	Train R^2	RMSE	MAE	SI	a20	Test R^2	RMSE	MAE	SI	a20	Ranking
ANN	0.959	0.140	0.113	0.086	0.984	0.932	0.190	0.148	0.111	0.921	4
BDT	0.934	0.178	0.140	0.108	0.929	0.915	0.212	0.167	0.123	0.889	5
KNN	0.979	0.100	0.078	0.061	0.976	0.958	0.149	0.115	0.086	0.952	1
LR	0.847	0.271	0.217	0.165	0.770	0.845	0.287	0.235	0.164	0.730	7
RFR	0.925	0.190	0.140	0.116	0.929	0.885	0.247	0.204	0.143	0.889	6
SVR	0.955	0.148	0.104	0.090	0.952	0.956	0.153	0.124	0.087	0.952	2
XG	0.999	0.023	0.017	0.014	1.000	0.919	0.207	0.158	0.119	0.841	3

The numbers indicate that the XGboost model accurately predicts the $f_{c\text{-gpm}}$ for the training datasets. However, during the testing of datasets, it was discovered that there were multiple instances (more than 15% of the data points) where the XGboost model exhibited deviations beyond the 20% error threshold. However, the KNN model demonstrated exceptional performance for both the training and testing datasets. The training datasets exhibited an R^2 of 0.979, which ranks second highest among the models tested, with XGboost being the only exception. Additionally, the R^2 value of 0.958 achieved by this model for testing datasets surpasses that of all other ML models evaluated. A comparable pattern was noted for other performance indicators as well. The SVR

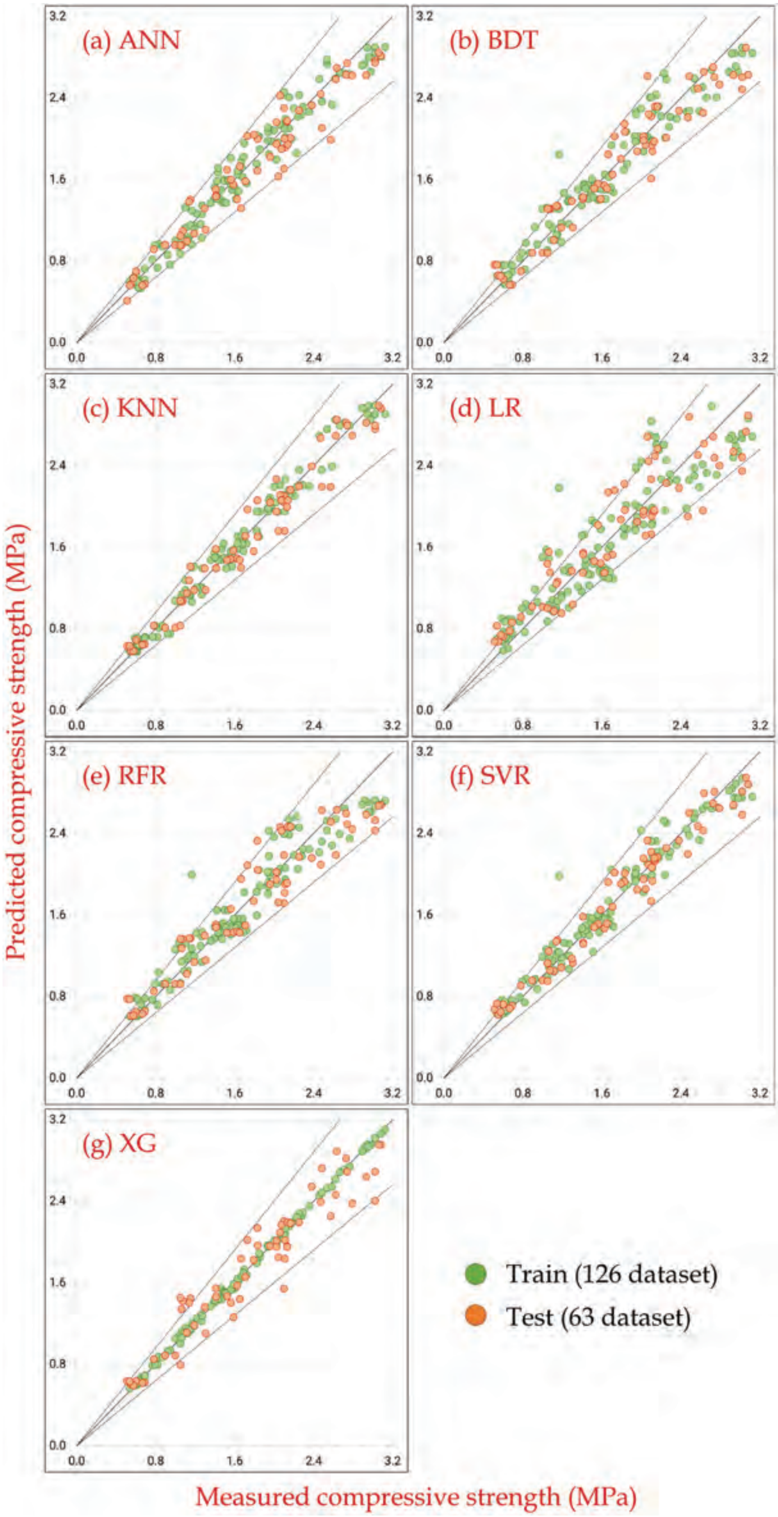

Figure 8. Predicted vs. measured compressive strength of geopolymer mortar for different machine-learning models (green dot: train dataset, red dot: test dataset, continues line: best-fit line between predicted and measured value, dot-dot line: 20% error envelope).

model demonstrated exceptional performance for both the training and testing datasets, with R^2 values of 0.955 and 0.956, respectively. Additionally, it is worth noting that both the KNN and SVR models exhibited a high level of accuracy in their predictions. Specifically, over 95% of the predicted values were within a 20% error margin for both the training and testing datasets.

As shown in Figure 9, the outcomes of cross-validation using K-fold validation are assessed using an R^2 and an RMSE. When compared to other machine learning models, the XGboost model has a higher R^2 and a lower RMSE for training dataset. The R^2 value for the training datasets for the XGboost model is almost unity for all folds. On the other hand, for testing datasets, it displays the range of 0.88 to 0.96 for R^2 value. For training datasets, every model has a limited range of variation in R^2 (the difference between the maximum and minimum R^2). However, for test datasets, this range within small limit only for ANN and KNN models. Because it is less than 0.05. The RMSE number also showed a similar pattern. The RMSE value of the XGboost model was 0.03 MPa for all folds for training datasets. However, for testing datasets, the RMSE varies from 0.15 to 0.24 MPa with the mean of 0.2 MPa. Considering both training and testing datasets, KNN models perform better than other models as RMSE for both cases, ranged between 0.11 to 0.15 MPa with mean of 0.13 MPa. These findings show that even though XGboost performed well in prediction model but have some overfitting issue. But KNN model not have an overfitting problem, and as a result, they are more trustworthy machine learning models for prediction.

Taylor diagrams are a visual representation that provides a straightforward means of evaluating the effectiveness of various ML models by examining the correlation between predicted values and observed values. To present a statistical comparison of many models, a two-dimensional graph is utilised to depict standard deviations, correlation coefficients, and root-mean-square discrepancies. The standard deviation is conventionally denoted as the radial distance between a data point and the origin in a Cartesian coordinate system. The root mean square error exhibits a direct relationship with the disparity, expressed in standard deviation units, between the observed and predicted values. The azimuthal angle is used to express the correlation coefficient. Figure 10 displays the Taylor diagrams representing the testing and training datasets.

The data presented in Figure 10 indicates that XGboost outperforms other models in the testing phase and exhibits a high degree of proximity to the observed value. However, in the testing phase, it exhibited superior performance only when compared to RFR and LR models. Although KNN and SVR exhibit a high degree of similarity and demonstrate comparable performance during the testing phase, it appears that KNN outperforms SVR in the training phase. In the current study, it was observed that KNN exhibited superior performance when compared to all other ML models, taking into account both the training and testing phases.

4.1. Error distribution

Figure 11 shows the error in the prediction of $f_{c\text{-gpm}}$ using various ML techniques. The error was calculated by the discrepancy between the predicted and measured values of $f_{c\text{-gpm}}$. The KNN model exhibits a relatively limited range of error distribution, spanning

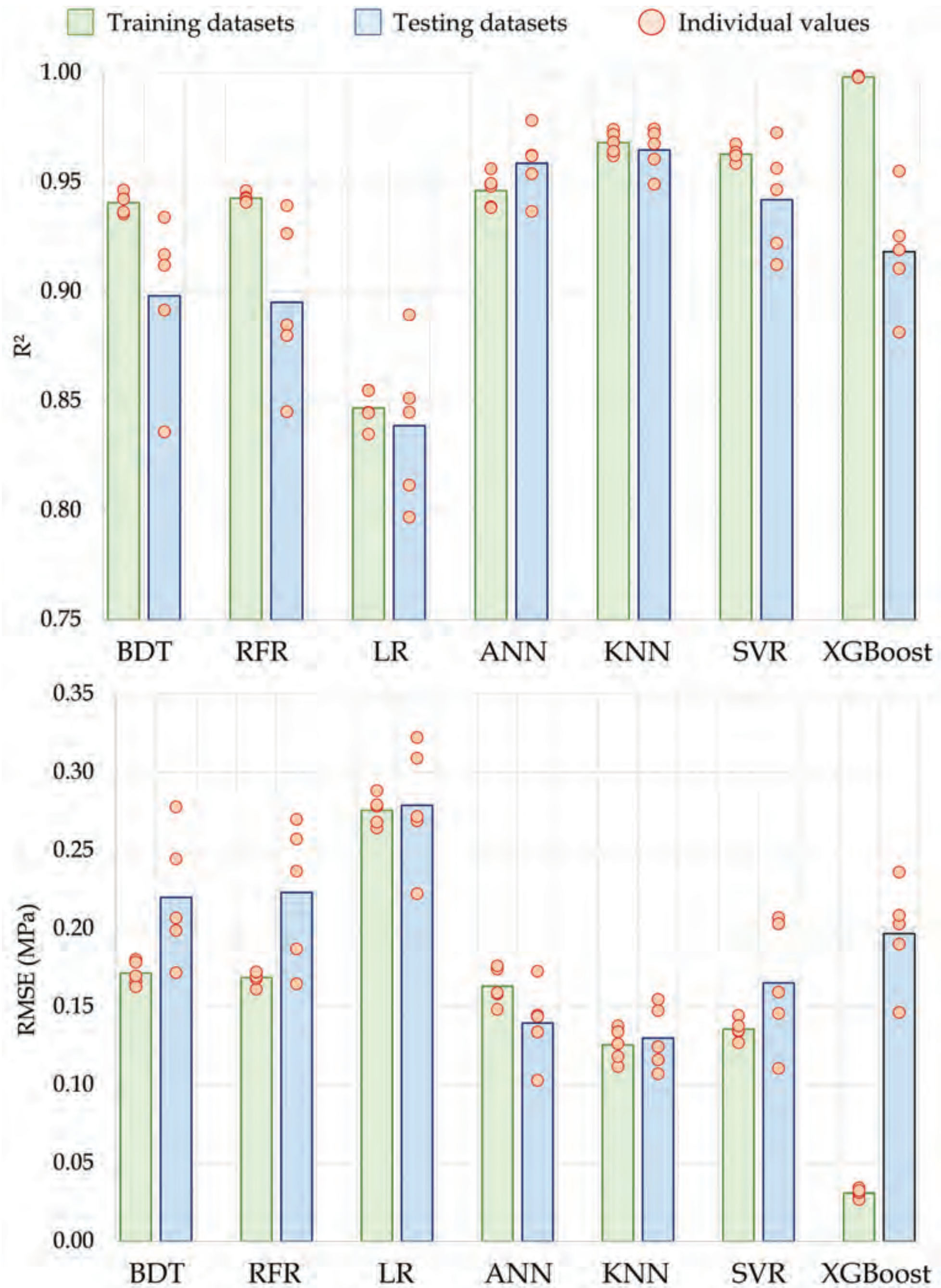

Figure 9. Five-fold validation for various machine learning models.

from −0.38 to 0.26 MPa. As anticipated, the linear regression (LR) model exhibits the most extensive spread of errors, spanning from −0.67 to 1.02 MPa.

All of the models exhibit errors that are evenly distributed on both sides, as the average error approaches zero. Moreover, it has been observed that KNN, XGboost and ANN

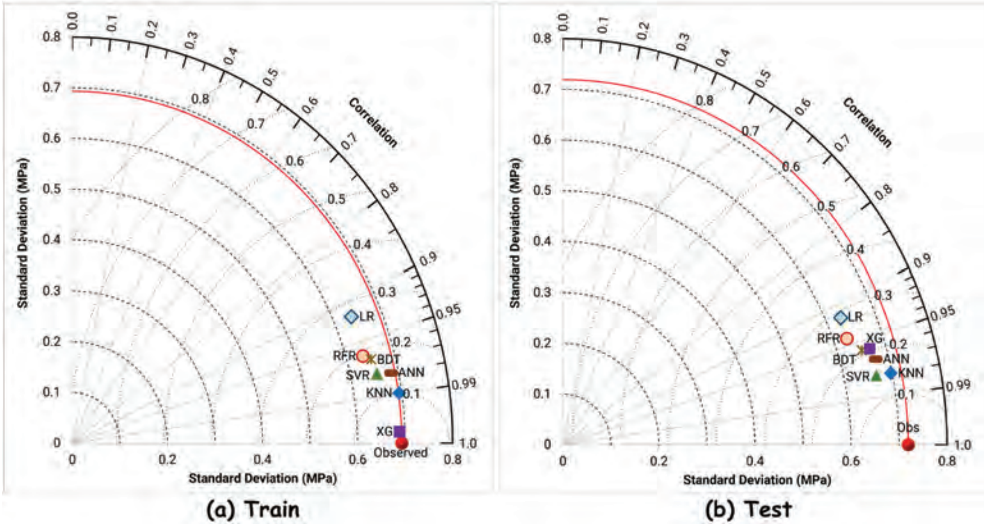

Figure 10. Taylor diagram for (a) training datasets and (b) test datasets. The diagrams offer a succinct statistical synopsis of the degree of similarity between prediction and observed datasets, as measured by their correlation, root-mean-square difference, and standard deviation. The point closer to the observed point (red mark in the horizontal axis) is the best model for prediction.

models demonstrate a tendency towards negative skewness, while other models tend to exhibit positive skewness. The ANN model exhibits a skewness value of −0.15, which is the lowest among the models considered. Conversely, the XGboost model demonstrates

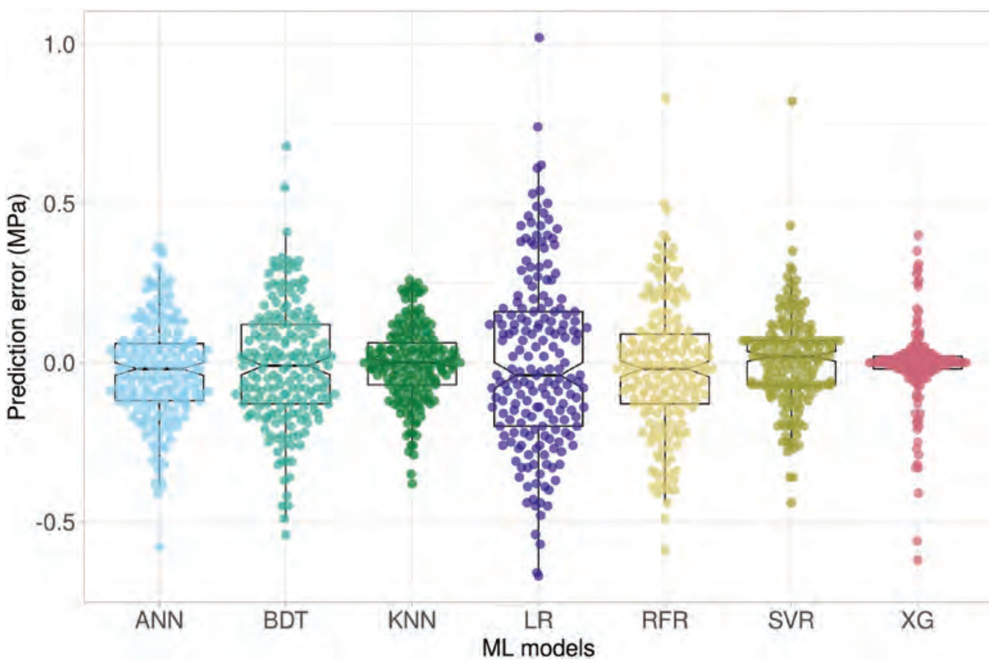

Figure 11. Quantitative comparison plots show the distribution of the errors for the seven machine learning methods.

the greatest skewness value of 1.07. The utilisation of various statistical and graphical techniques has the potential to greatly enhance the evaluation of prediction models. This suggests that employing a diverse range of statistical indicators and visual representations to evaluate the effectiveness of prediction models could yield a more comprehensive analysis.

4.2. Sensitivity analysis

Machine learning models may sometimes demonstrate opaque behaviour as a result of their complex structure [78]. The use of SHAP (Shapley Additive Explanations) has shown significant benefits in the analysis of complex machine-learning models that include a wide array of factors [79,80]. As KNN has shown excellent performance in the prediction of $f_{c\text{-gpm}}$, therefore, the KNN model was used for SHAP analysis.

Figure 12(a) illustrates the average SHAP values about different qualities, which serve as the independent variables, about the predictions of $f_{c\text{-gpm}}$. The aforementioned

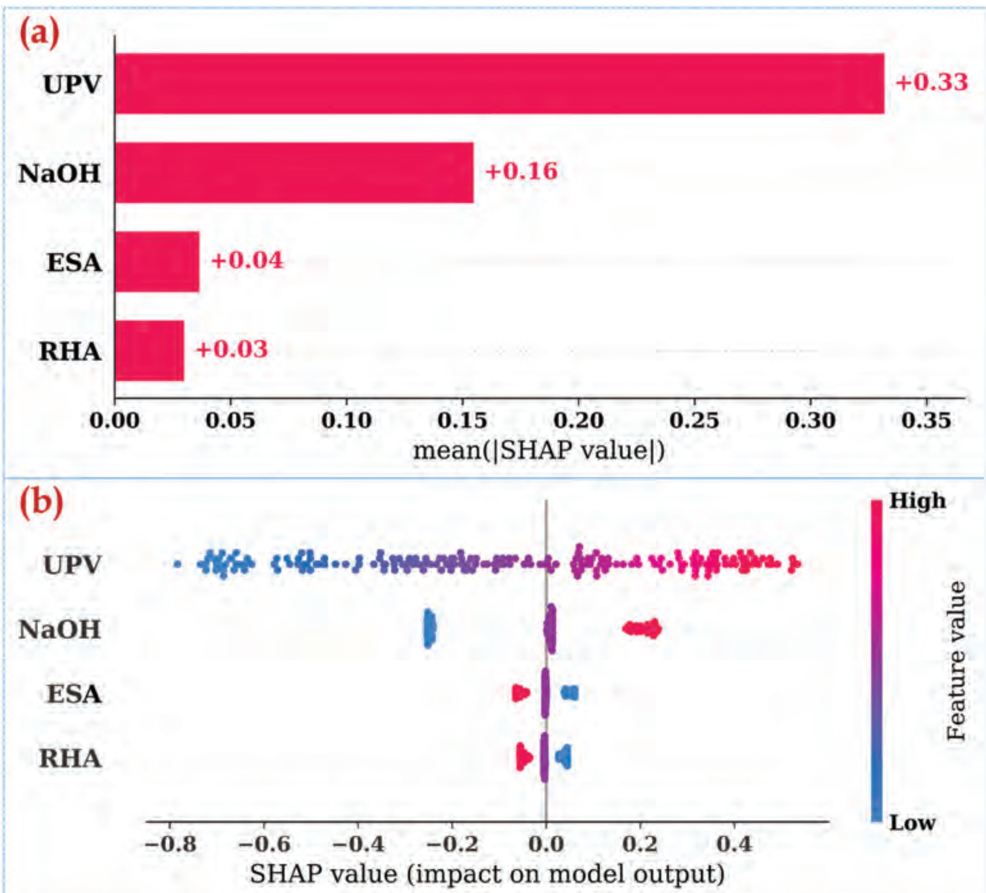

Figure 12. SHAP summary plot of the feature importance on the prediction of KNN model. (a) mean SHAP value and (b) SHAP summary plot for each independent parameter. The SHAP values (horizontal axis) represent the contribution of each parameter (vertical axis). Features are ordered according to importance.

predictions are generated from the KNN model. Based on the results obtained, it is apparent that the UPV demonstrates the greatest SHAP value, hence showing its substantial impact on the prediction of $f_{c\text{-gpm}}$. Simultaneously, it was noted that the content of the ESA and RHA had the lowest SHAP value, indicating comparatively little influence on the prediction of $f_{c\text{-gpm}}$.

The visual representation in Figure 12(b) illustrates the beeswarm plot used for predicting $f_{c\text{-gpm}}$. The plot shows that lower values of UPV are associated with negative SHAP values, as evidenced by the progressively blue spots stretching towards the left. On the other hand, it can be observed that higher values of UPV exhibit positive SHAP values, as indicated by the increasing red colouration of the points extending towards the left. This observation suggests that there is a positive correlation between the UPV and the predicted $f_{c\text{-gpm}}$ value. Lower content of ESA and RHA results in increased prediction of $f_{c\text{-gpm}}$.

The latter phase of this study involves evaluating the resilience of the KNN model that was created to forecast the compressive strength using the specified input variables, particularly when UPV is missing. This study is crucial, particularly in industrial settings where a UPV cannot be directly measured. Figure 13 provides a Performance Indexes of the model's performance, considering UPV as input variable or not. As anticipated, input variables with UPV yielded the highest R^2 value (average of 0.97 for training datasets and 0.96 for testing datasets) and low RMSE value (average of 0.13 MPa for both training and testing dataset). Although, input variables without UPV yielded the high R^2 value and low RMSE, still it is poor than input variable with UPV. Also, when variable without UPV is considered, it shown that R^2 and RMSE value for each fold is more scatter.

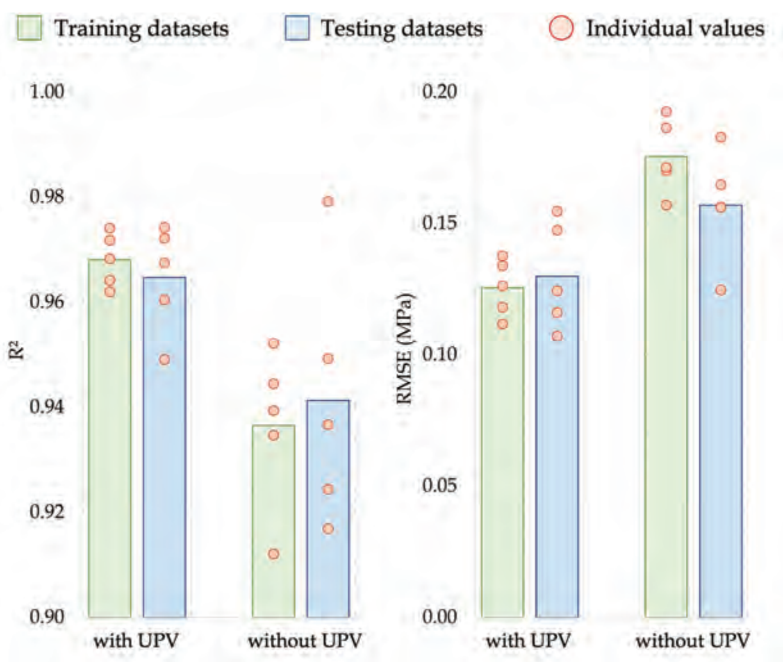

Figure 13. Performance indexes (R^2 and RMSE) of the KNN model for input variables include with UPV and without UPV.

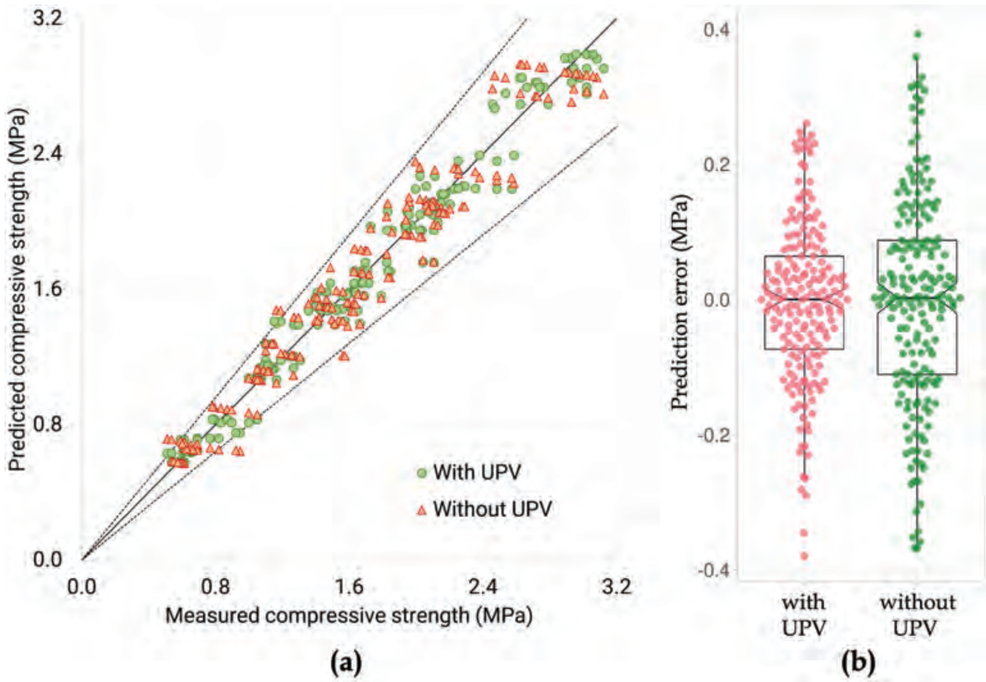

Figure 14. Effect of input variables (a) predicted vs. measured compressive strength values and (b) error distribution.

Figure 14 displays the results of comparing predicted and measured values and error distribution for the prediction using input variable with and without UPV. Although, predicted and measured compressive strength graph is not provide much visual deficiency, UPV as input variable influence is further supported by the error distribution. It shows some variability in model performance. These results shown that, omitting the variable UPV led to a relatively some decrease in accuracy.

5. Conclusion

This study proposes a framework for predicting the $f_{c\text{-gpm}}$ using ML techniques. Twenty-seven mix designs consisting of various combinations of ESA, RHA and NaOH content with 189 experimental datasets were used to train and test the models. The main findings of the study are:

- The statistical analyses show that there is a moderate correlation between UPV and $f_{c\text{-gpm}}$ with an R^2 of 0.833.
- Amongst the ML models evaluated in this study, the KNN model performed best for predicting $f_{c\text{-gpm}}$. The accuracy of $R^2 = 0.979$ and RMSE = 0.1 MPa for training datasets and $R^2 = 0.958$ and RMSE = 0.149 MPa for testing datasets, respectively.
- The feature importance analysis with SHAP indicates that the most significant parameter influencing the prediction of the $f_{c\text{-gpm}}$ is UPV.

The present work provides a systematic evaluation of predicting $f_{c\text{-}gpm}$, which can provide the knowledge base and be useful in the real world. The application of geopolymer technology, which incorporates environmentally sustainable alternatives including ESA, RHA, and quarry waste, coupled with caustic soda as an alkaline activator, shows potential for reducing carbon dioxide emissions in the construction sector. The utilisation of ESA, RHA, and quarry waste in the construction industry might augment their worth as feasible construction materials, hence alleviating their classification as mere waste byproducts. The ability to forecast the compressive strength of geopolymer mortar can aid in refining the composition of geopolymer mortar made from quarry waste. This can be achieved by modifying the type and proportion of precursors and alkaline activators. Additionally, it can aid in diminishing the duration and expenses associated with experimental testing and quality assurance of geopolymer mortar derived from quarry waste. Material scientists and designers can use reliable prediction models to select the optimal input variables and the suitable mix parameters for producing geopolymer mortar with the desired properties.

Disclosure statement

No potential conflict of interest was reported by the author(s).

References

[1] Sathiparan N, De Zoysa HTSM. The effects of using agricultural waste as partial substitute for sand in cement blocks. J Buil Eng. 2018;19:216–227. doi: 10.1016/j.jobe.2018.04.023
[2] Sathiparan N. Performance of sustainable cement mortar containing different types of masonry construction and demolition wastes. Clean Technol Envir. 2023 doi: 10.1007/s10098-023-02681-2
[3] Yogananth Y, Thanushan K, Sangeeth P, et al. Comparison of strength and durability properties between earth-cement blocks and cement–sand blocks. Innov Infrastruct Solut. 2019;4(1):50. doi: https://doi.org/10.1007/s41062-019-0238-8
[4] Shen W, Yang Z, Cao L, et al. Characterization of manufactured sand: particle shape, surface texture and behavior in concrete. Constr Build Mater. 2016;114:595–601. doi: 10.1016/j.conbuildmat.2016.03.201
[5] Gonçalves JP, Tavares LM, Toledo Filho RD, et al. Comparison of natural and manufactured fine aggregates in cement mortars. Cement Concr Res. 2007;37(6):924–932. doi: 10.1016/j.cemconres.2007.03.009
[6] Donza H, Cabrera O, Irassar EF. High-strength concrete with different fine aggregate. Cement Concr Res. 2002;32(11):1755–1761. doi: 10.1016/S0008-8846(02)00860-8
[7] Nanthagopalan P, Santhanam M. Fresh and hardened properties of self-compacting concrete produced with manufactured sand. Cem Concr Compos. 2011;33(3):353–358. doi: 10.1016/j.cemconcomp.2010.11.005
[8] Benabed B, Kadri E-H, Azzouz L, et al. Properties of self-compacting mortar made with various types of sand. Cem Concr Compos. 2012;34(10):1167–1173. doi: 10.1016/j.cemconcomp.2012.07.007
[9] Mahakavi P, Chithra R, Kavitha K. Effect of recycled coarse aggregate and foundry sand on the properties of self-compacting concrete. Mag Concr Res. 2019;71(9):449–460. doi: 10.1680/jmacr.17.00455
[10] Sundaralingam K, Peiris A, Anburuvel A, et al. Quarry dust as river sand replacement in cement masonry blocks: effect on mechanical and durability characteristics. Materialia. 2022;21:101324. doi: 10.1016/j.mtla.2022.101324

[11] Sathiparan N, Jaasim JHM, Banujan B. Sustainable production of cement masonry blocks with the combined use of fly ash and quarry waste. Materialia. 2022;26:101621. doi: 10.1016/j.mtla.2022.101621
[12] Subramaniam DN, Sathiparan N. Comparative study of fly ash and rice husk ash as cement replacement in pervious concrete: mechanical characteristics and sustainability analysis. International Journal Of Pavement Engineering. 2022;24(2):1–18. doi: 10.1080/10298436.2022.2075867
[13] Davidovits J, Sawyer J. Early high-strength mineral polymer. United States Patent No: US4509985A. 1985.
[14] Silverstrim T, Rostami H, Larralde J, et al. Fly ash cementitious material and method of making a product. United States Patent No: US5601643A. 1997.
[15] Van Jaarsveld JGS, Van Deventer JSJ, Lorenzen L. The potential use of geopolymeric materials to immobilise toxic metals: Part I. Theory and applications. Miner Eng. 1997;10(7):659–669. doi: 10.1016/S0892-6875(97)00046-0
[16] Naskar S, Chakraborty AK. Effect of nano materials in geopolymer concrete. Perspect Sci. 2016;8:273–275. doi: 10.1016/j.pisc.2016.04.049
[17] Talakokula V, Vaibhav SB. Non-destructive strength evaluation of fly ash based geopolymer concrete using piezo sensors. Procedia Eng. 2016;145:1029–1035. doi: 10.1016/j.proeng.2016.04.133
[18] Chithambaram SJ, Kumar S, Prasad MM, et al. Effect of parameters on the compressive strength of fly ash based geopolymer concrete. Struct Concr. 2018;19(4):1202–1209. doi: 10.1002/suco.201700235
[19] Amran M, Al-Fakih A, Chu SH, et al. Long-term durability properties of geopolymer concrete: an in-depth review. Case Studies Construction Mater. 2021;15:e00661. doi: 10.1016/j.cscm.2021.e00661
[20] Cristelo N, Glendinning S, Miranda T, et al. Soil stabilisation using alkaline activation of fly ash for self compacting rammed earth construction. Constr Build Mater. 2012;36:727–735. doi: 10.1016/j.conbuildmat.2012.06.037
[21] Lemougna PN, Madi AB, Kamseu E, et al. Influence of the processing temperature on the compressive strength of Na activated lateritic soil for building applications. Constr Build Mater. 2014;65:60–66. doi: 10.1016/j.conbuildmat.2014.04.100
[22] Petrillo A, Cioffi R, Ferone C, et al. Eco-sustainable geopolymer concrete blocks production process. Agric Agric Sci Procedia. 2016;8:408–418. doi: 10.1016/j.aaspro.2016.02.037
[23] Komnitsas KA. Potential of geopolymer technology towards green buildings and sustainable cities. Procedia Eng. 2011;21:1023–1032. doi: 10.1016/j.proeng.2011.11.2108
[24] Posi P, Teerachanwit C, Tanutong C, et al. Lightweight geopolymer concrete containing aggregate from recycle lightweight block. Materials & Design (1980-2015). 2013;52:580–586. doi: 10.1016/j.matdes.2013.06.001
[25] Assaedi H, Shaikh FUA, Low IM. Effect of nano-clay on mechanical and thermal properties of geopolymer. J Asian Ceram Soc. 2016;4(1):19–28. doi: 10.1016/j.jascer.2015.10.004
[26] Anburuvel A, Sathiparan N, Dhananjaya GMA, et al. Characteristic evaluation of geopolymer based lateritic soil stabilization enriched with eggshell ash and rice husk ash for road construction: an experimental investigation. Constr Build Mater. 2023;387:131659. doi: 10.1016/j.conbuildmat.2023.131659
[27] Brahimi A, Meghachou M, Abbad H, et al. Analysis of experimental data of environmental cement prepared by fly ash of eggs shell and sand dune for reduction of carbon dioxid. Data Brief. 2020;30:105407. doi: 10.1016/j.dib.2020.105407
[28] Hwang C-L, Huynh T-P. Effect of alkali-activator and rice husk ash content on strength development of fly ash and residual rice husk ash-based geopolymers. Constr Build Mater. 2015;101:1–9. doi: 10.1016/j.conbuildmat.2015.10.025
[29] Karim MR, Zain MFM, Jamil M, et al. Development of a zero-cement binder using slag, fly ash, and rice husk ash with chemical activator. Adv Mater Sci Eng. 2015;2015:1–14. doi: 10.1155/2015/247065

[30] Poorveekan K, Ath KMS, Anburuvel A, et al. Investigation of the engineering properties of cementless stabilized earth blocks with alkali-activated eggshell and rice husk ash as a binder. Constr Build Mater. 2021;277:122371. doi: 10.1016/j.conbuildmat.2021.122371
[31] Tchakouté HK, Tchinda Mabah DE, Henning Rüscher C, et al. Preparation of low-cost nano and microcomposites from chicken eggshell, nano-silica and rice husk ash and their utilisations as additives for producing geopolymer cements. J Asian Ceram Soc. 2020;8(1):149–161. doi: 10.1080/21870764.2020.1718860
[32] Mayooran S, Ragavan S, Sathiparan N. Comparative study on open air burnt low- and high-carbon rice husk ash as partial cement replacement in cement block production. J Buil Eng. 2017;13:137–145. doi: 10.1016/j.jobe.2017.07.011
[33] Seevaratnam V, Uthayakumar D, Sathiparan N. Influence of Rice huskash on characteristics of earth cement blocks. MRS Adv. 2020;5(54):2793–2805. doi: 10.1557/adv.2020.294
[34] Sathiparan N, Anjalee WAV, Kandage KKS. The scale effect on small-scale modelling of cement block masonry. Mater Struct. 2016;49(7):2935–2946. doi: 10.1617/s11527-015-0696-1
[35] Ivanchev I. Investigation with non-destructive and destructive methods for assessment of concrete compressive strength. Appl Sci. 2022;12(23):12172. doi: 10.3390/app122312172
[36] Saleh E, Tarawneh A, Dwairi H, et al. Guide to non-destructive concrete strength assessment: homogeneity tests and sampling plans. J Buil Eng. 2022;49:104047. doi: 10.1016/j.jobe.2022.104047
[37] Sathiparan N, Jeyananthan P. Predicting compressive strength of cement-stabilized earth blocks using machine learning models incorporating cement content, ultrasonic pulse velocity, and electrical resistivity. Case Stud NondestrTest Eval. 2023;1–25. doi: 10.1080/10589759.2023.2240940
[38] Sathiparan N, Jayasundara WGBS, Samarakoon KSD, et al. Prediction of characteristics of cement stabilized earth blocks using non-destructive testing: ultrasonic pulse velocity and electrical resistivity. Materialia. 2023;29:101794. doi: 10.1016/j.mtla.2023.101794
[39] Singh N, Singh SP. Evaluating the performance of self compacting concretes made with recycled coarse and fine aggregates using non destructive testing techniques. Constr Build Mater. 2018;181:73–84. doi: 10.1016/j.conbuildmat.2018.06.039
[40] Shakr Piro N, Mohammed A, Hamad SM, et al. Electrical resistivity-compressive strength predictions for normal strength concrete with waste steel slag as a coarse aggregate replacement using various analytical models. Constr Build Mater. 2022;327:127008. doi: 10.1016/j.conbuildmat.2022.127008
[41] Yılmaz T, Ercikdi B. Predicting the uniaxial compressive strength of cemented paste backfill from ultrasonic pulse velocity test. Case Stud NondestrTest Eval. 2016;31(3):247–266. doi: 10.1080/10589759.2015.1111891
[42] Jiang H, Han J, Li Y, et al. Relationship between ultrasonic pulse velocity and uniaxial compressive strength for cemented paste backfill with alkali-activated slag. Case Stud NondestrTest Eval. 2020;35(4):359–377. doi: 10.1080/10589759.2019.1679140
[43] Selcuk S, Tang P. A metaheuristic-guided machine learning approach for concrete strength prediction with high mix design variability using ultrasonic pulse velocity data. Dev Built Environ. 2023;15:100220. doi: 10.1016/j.dibe.2023.100220
[44] Mata R, Ruiz RO, Nuñez E. Correlation between compressive strength of concrete and ultrasonic pulse velocity: a case of study and a new correlation method. Constr Build Mater. 2023;369:130569. doi: 10.1016/j.conbuildmat.2023.130569
[45] Estévez E, Martín DA, Argiz C, et al. Ultrasonic pulse velocity—compressive strength relationship for Portland cement mortars cured at different conditions. Crystals. 2020;10(2):133. doi: 10.3390/cryst10020133
[46] Silva SDCD, Sivahar V. Non-destructive evaluation of strength gain of ordinary Portland cement mortar by ultrasonic pulse velocity method. 2016 Moratuwa Engineering Research Conference (MERCon); Colomb, SriLanka. 2016, pp. 337–342.
[47] Sathiparan N, Jeyananthan P. Predicting compressive strength of cement-stabilized earth blocks using machine learning models incorporating cement content, ultrasonic pulse

velocity, and electrical resistivity. Case Stud Nondestr Test Eval. 2018:1–25. doi: 10.1080/10589759.2023.2240940
[48] Abdelhedi M, Jabbar R, Mnif T, et al. Ultrasonic velocity as a tool for geotechnical parameters prediction within carbonate rocks aggregates. Arabian J Geosci. 2020;13(4):180. doi: 10.1007/s12517-020-5070-0
[49] Mohammed T, Ghanizadeh A, Clarkson CR, et al. Profile ultrasonic velocity measurements performed on slabbed core: implications for high-resolution permeability prediction in low-permeability rocks. SPE Canadian Energy Technology Conference; 2022 Mar 16–17; Calgary, Alberta, Canada. 2022, p. D011S002R003.
[50] Abdelhedi M, Abbes C, Preliminary artificial neural network modeling predicting uniaxial compressive strength within carbonate rocks. 2nd International Conference on Advances in Rock Mechanics - TuniRock 2022; Mar 25–27 2022; Hamammet, Tunisia. 2022, pp. ISRM-TUNIROCK-2022–020.
[51] Abdelhedi M, Jabbar R, Said AB, et al. Machine learning for prediction of the uniaxial compressive strength within carbonate rocks. Earth Sci Inform. 2023;16(2):1473–1487. doi: 10.1007/s12145-023-00979-9
[52] Abdelhedi M, Abbes C. Study of physical and mechanical properties of carbonate rocks and their applications on georesources exploration in Tunisia. Carbonates Evaporites. 2021;36(2):35. doi: 10.1007/s13146-021-00688-8
[53] Ahmad A, Ahmad W, Aslam F, et al. Compressive strength prediction of fly ash-based geopolymer concrete via advanced machine learning techniques. Case Stud Constr Mater. 2022;16:e00840. doi: 10.1016/j.cscm.2021.e00840
[54] Zhang LV, Marani A, Nehdi ML. Chemistry-informed machine learning prediction of compressive strength for alkali-activated materials. Constr Build Mater. 2022;316:126103. doi: 10.1016/j.conbuildmat.2021.126103
[55] Wu J, Jing H, Yin Q, et al. Strength prediction model considering material, ultrasonic and stress of cemented waste rock backfill for recycling gangue. J Clean Prod. 2020;276:123189. doi: 10.1016/j.jclepro.2020.123189
[56] Bilgehan M. A comparative study for the concrete compressive strength estimation using neural network and neuro-fuzzy modelling approaches. Case Stud Nondestr Test Eval. 2011;26(1):35–55. doi: 10.1080/10589751003770100
[57] Vidya Sagar R, Dutta M. Combined usage of acoustic emission technique and ultrasonic pulse velocity test to study crack classification in reinforced concrete structures. Case Stud Nondestr Test Eval. 2021;36(1):62–96. doi: 10.1080/10589759.2019.1692013
[58] Asteris PG, Lourenço PB, Hajihassani M, et al. Soft computing-based models for the prediction of masonry compressive strength. Eng Struct. 2021;248:113276. doi: 10.1016/j.engstruct.2021.113276
[59] Sharafati A, Haji Seyed Asadollah SB, Al-Ansari N. Application of bagging ensemble model for predicting compressive strength of hollow concrete masonry prism. Ain Shams Eng. 2021;12(4):3521–3530. doi: 10.1016/j.asej.2021.03.028
[60] Lan G, Wang Y, Zeng G, et al. Compressive strength of earth block masonry: estimation based on neural networks and adaptive network-based fuzzy inference system. Compos Struct. 2020;235:111731. doi: 10.1016/j.compstruct.2019.111731
[61] Asteris PG, Skentou AD, Bardhan A, et al. Soft computing techniques for the prediction of concrete compressive strength using non-destructive tests. Constr Build Mater. 2021;303:124450. doi: 10.1016/j.conbuildmat.2021.124450
[62] Khashman A, Akpinar P. Non-destructive prediction of concrete compressive strength using neural networks. Procedia Comput Sci. 2017;108:2358–2362. doi: 10.1016/j.procs.2017.05.039
[63] El-Mir A, El-Zahab S, Sbartaï ZM, et al. Machine learning prediction of concrete compressive strength using rebound hammer test. J Buil Eng. 2023;64:105538. doi: 10.1016/j.jobe.2022.105538
[64] Li D, Tang Z, Kang Q, et al. Machine learning-based method for predicting compressive strength of concrete. Processes. 2023;11(2):390. doi: 10.3390/pr11020390

[65] Cree D, Rutter A. Sustainable bio-inspired limestone eggshell powder for potential industrialized applications. ACS Sustain Chem Eng. 2015;3(5):941–949. doi: 10.1021/acssuschemeng.5b00035

[66] Witoon T. Characterization of calcium oxide derived from waste eggshell and its application as CO2 sorbent. Ceram Int. 2011;37(8):3291–3298. doi: 10.1016/j.ceramint.2011.05.125

[67] Cree D, Pliya P. Effect of elevated temperature on eggshell, eggshell powder and eggshell powder mortars for masonry applications. J Buil Eng. 2019;26:100852. doi: 10.1016/j.jobe.2019.100852

[68] ASTM-C109. Standard test method for compressive strength of hydraulic cement mortars (using 2-in. Or [50 mm] cube specimens). West Conshohocken, PA: ASTM International; 2020.

[69] ASTM-C597. Standard test method for pulse velocity through concrete. West Conshohocken, PA: ASTM International; 2010.

[70] Sathiparan N, Jeyananthan P, Subramaniam DN. Effect of aggregate size, aggregate to cement ratio and compaction energy on ultrasonic pulse velocity of pervious concrete: prediction by an analytical model and machine learning techniques. Asian J Civ Eng. 2023;25(1):495–509. doi: 10.1007/s42107-023-00790-3

[71] Carrasco EVM, Silva SR, Mantilla JNR. Assessment of mechanical properties and the influence of the addition of sawdust in soil–cement bricks using the technique of ultrasonic anisotropic inspection. J Mater Civ Eng. 2014;26(2):219–225. doi: 10.1061/(ASCE)MT.1943-5533.0000723

[72] Abdelhedi M, Aloui M, Mnif T, et al. Ultrasonic velocity as a tool for mechanical and physical parameters prediction within carbonate rocks. Geomech Eng. 2017;13(3):371–384. doi: 10.12989/GAE.2017.13.3.371

[73] Mohamed A, Thameur M, Chedly A. Ultrasonic velocity as a tool for physical and mechanical parameters prediction within geo-materials: application on cement mortar. Russ J Nondestr Test. 2018;54(5):345–355. doi: 10.1134/S1061830918050091

[74] Subramaniam DN, Jeyananthan P, Sathiparan N. Soft computing techniques to predict the electrical resistivity of pervious concrete. Asian J Civ Eng. 2023;25(1):711–722. doi: 10.1007/s42107-023-00806-y

[75] Sathiparan N, Jeyananthan P. Prediction of masonry prism strength using machine learning technique: effect of dimension and strength parameters. Mater Today Commun. 2023;35:106282. doi: 10.1016/j.mtcomm.2023.106282

[76] Armaghani DJ, Asteris PG. A comparative study of ANN and ANFIS models for the prediction of cement-based mortar materials compressive strength. Neural Comput Appl. 2021;33(9):4501–4532. doi: 10.1007/s00521-020-05244-4

[77] Asteris PG, Douvika MG, Karamani CA, et al. A novel heuristic algorithm for the modeling and risk assessment of the COVID-19 pandemic phenomenon. Comput Model Eng Sci. 2020;125(2):815–828. doi: 10.32604/cmes.2020.013280

[78] Shah SFA, Chen B, Zahid M, et al. Compressive strength prediction of one-part alkali activated material enabled by interpretable machine learning. Constr Build Mater. 2022;360:129534. doi: 10.1016/j.conbuildmat.2022.129534

[79] Zhang J, Niu W, Yang Y, et al. Machine learning prediction models for compressive strength of calcined sludge-cement composites. Constr Build Mater. 2022;346:128442. doi: 10.1016/j.conbuildmat.2022.128442

[80] Quan Tran V, Quoc Dang V, Si Ho L. Evaluating compressive strength of concrete made with recycled concrete aggregates using machine learning approach. Constr Build Mater. 2022;323:126578. doi: 10.1016/j.conbuildmat.2022.126578